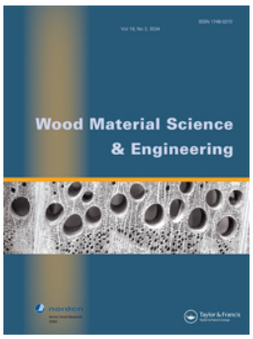

Wood Material Science & Engineering

ISSN: (Print) (Online) Journal homepage: www.tandfonline.com/journals/swoo20

Effect of thermal modification of wood on the rheology, mechanical properties and dimensional stability of wood composite filaments and 3D-printed parts

Daša Krapež Tomec, Manfred Schöflinger, Jürgen Leßlhumer, Jure Žigon, Miha Humar & Mirko Kariž

To cite this article: Daša Krapež Tomec, Manfred Schöflinger, Jürgen Leßlhumer, Jure Žigon, Miha Humar & Mirko Kariž (15 Feb 2024): Effect of thermal modification of wood on the rheology, mechanical properties and dimensional stability of wood composite filaments and 3D-printed parts, Wood Material Science & Engineering, DOI: 10.1080/17480272.2024.2316740

To link to this article: https://doi.org/10.1080/17480272.2024.2316740

Published online: 15 Feb 2024.

WOOD MATERIAL SCIENCE & ENGINEERING
https://doi.org/10.1080/17480272.2024.2316740

Taylor & Francis
Taylor & Francis Group

ORIGINAL ARTICLE

Effect of thermal modification of wood on the rheology, mechanical properties and dimensional stability of wood composite filaments and 3D-printed parts

Daša Krapež Tomec [a], Manfred Schöflinger[b], Jürgen Leßlhumer[b], Jure Žigon [a], Miha Humar [a] and Mirko Kariž [a]

[a]Biotechnical Faculty, University of Ljubljana, Ljubljana, Slovenia; [b]Kompetenzzentrum Holz GmbH, Linz, Austria

ABSTRACT

This study investigates the effects of thermal modification (TM) on wood-filled polylactic acid composite filaments for 3D printing. Nine composite formulations with different wood content were analysed. The wood particles came from unmodified and thermally modified beech wood (180 °C or 200 °C). The results showed that the incorporation of thermally modified (TMd) wood changed the filament properties, resulting in lower density and reduced surface roughness. The 3D-printed parts with TMd wood particles had a higher water contact angle, higher storage modulus, lower glass transition temperature, higher modulus of elasticity and higher indentation hardness. However, the tensile strength of the 3D-printed parts decreases, even though the results of parts with TMd wood showed higher strength compared to unmodified wood at the same filler content. Surprisingly, TMd wood had no effect on water absorption under humid conditions. Scanning electron micrographs showed improved interfacial adhesion between TMd wood particles and PLA, with smaller voids in the filament compared to filaments with unmodified wood particles. The study suggests that further research into use of TMd wood particles in composite holds promise for environmentally friendly 3D printing materials with favourable thermal and mechanical properties, impacting the expanding market for sustainable solutions in 3D printing.

ARTICLE HISTORY
Received 12 December 2023
Revised 31 January 2024
Accepted 6 February 2024

KEYWORDS
Wood-polylactic acid composite; 3D printing; thermally modified wood; dimensional stability; mechanical properties

1. Introduction

In recent years, materials research for low-cost extrusion-based 3D printers has gained acceptance. Technologies generally used in 3D printing include fused filament fabrication (FFF), in which a polymer material is extruded layer by layer to form a 3D object. FFF-based 3D printing is a widely used additive manufacturing technology with thermoplastic materials. For the printing process, a pre-prepared filament is fed into the 3D printer, in which the polymer filament is melted and extruded from a temperature-controlled nozzle onto a build platform. The object is created by layering thermoplastic with either the nozzle or the build platform moving in the x-, y- and z-axes (Rajendran Royan *et al*. 2021). Despite many advantages, one of the disadvantages of this technique is that the quality and mechanical properties (tensile strength, flexural strength and impact strength) of the printed product are not excellent, mainly due to the layering technique used in printing, which involves more contact points/failures, and the inevitable presence of voids. In addition, the mechanical properties of 3D-printed objects are anisotropic and strongly depend on the processing parameters (Mazzanti *et al*. 2019).

Composite filaments containing a number of different synthetic and natural fillers have been developed. One optional natural filler is wood flour, which is a by-product of the wood processing industry and has the advantage of low density, high stiffness, biodegradability, and low costs (Liu *et al*. 2017). The addition of wood flour to PLA can reduce the cost of composites and contribute to their sustainability and appearance. The technology is commercially available, and the use of wood-plastic filaments is based on their aesthetics. The current focus is on improving their properties.

An inhomogeneous mix between filler and polymer matrix, temperature control, and the formation of voids during processing lead to problems such as clogging of the nozzle in a 3D printer and inconsistent mechanical performance. To improve mixing and interfacial bonding between matrices and fillers, additives such as coupling agents (Mazzanti *et al*. 2019), chemical treatment (Stoof *et al*. 2017), and compatibilisers (Guo *et al*. 2018) are added. In addition, the effect of processing parameters and printing parameters has not been thoroughly researched until recently.

The percentage of wood in previous studies rarely exceeds 30% by mass. Higher fibre content ultimately leads to more complex printing in the 3D printer, such as an inhomogeneous natural-fibre-reinforced composite mixture that can lead to nozzle clogging and higher melt viscosity that requires a higher extrusion power. In addition, lower polymer matrices could result in a more brittle filament due to a decrease in the polymer content matrix that can enclose the fibres (Nguyen *et al*. 2018).

Wood particles affect the thermal stability of 3D-printed parts, resulting in a lower thermal decomposition temperature

CONTACT Mirko Kariž mirko.kariz@bf.uni-lj.si Biotechnical Faculty, University of Ljubljana, Jamnikarjeva 101, Ljubljana 1000, Slovenia

(Tao *et al*. 2017). The glass transition temperature depends on the compatibility of the particles in the composite, and fillers reduce the compatibility of the composite, leading to a lower glass transition temperature (Lee *et al*. 2008). Therefore, the glass transition temperature is lowered by the poor compatibility between wood and PLA (Tao *et al*. 2017).

Interest in sustainable materials is growing exponentially due to environmental concerns. To counteract this, innovative solutions such as wood composites in 3D printing are becoming increasingly important. This interest stems from a desire to reduce the impact on the environment and promote environmentally friendly alternatives in the manufacturing process. Wood composites are a renewable resource that offers a balance between material strength and sustainability, making them a promising choice for the advancement of green technologies such as 3D printing. Nevertheless, there is a knowledge gap regarding the performance and compatibility of thermally modified wood particles and PLA that could significantly upgrade the field of wood composites and the overall feasibility of integrating this material. It could contribute to the development of wood-polymer composites with improved mechanical properties and better performance in various applications.

The objective of this work is to investigate the effects of TM of wood particles on the properties of wood-filled PLA composite filaments for an application in a fused filament fabrication 3D printing application. Thermal and mechanical properties, dimensional stability and hydrophobicity were determined on obtained filaments and 3D printed parts.

2. Materials

The research was divided into five main parts: 1) preparation of wood-polymer composite filaments and 3D-printed test specimens, 2) measurement of dimensional stability of 3D-printed parts, 3) analysis of the mechanical properties of 3D-printed parts, 4) analysis of the rheological properties of 3D-printed parts, and 5) SEM micrographs of filaments and of 3D-printed parts.

In the present study, the PLA type Ingeo™ 2003D (NatureWorks, Blair, Nebraska, USA) in granular form was used as the base material. The melt temperature of the material is 210 °C, tensile strength at break 53 MPa (ASTM D882), specific gravity 1.24 g × cm^{-3} (ASTM D792), melt flow index 6 g × 10 min–1 at 210 °C (ASTM D1238).

For PLA reinforcement, beech (*Fagus sylvatica* L.) wood flour was prepared in three different variations: unmodified beech wood, beech wood thermally modified at 180 °C, and beech wood thermally modified at 200 °C. Modification was performed according to the Silvapro procedure in semi-anoxic conditions (Rep *et al*. 2012). To improve the compatibility between the PLA polymer and the wood, TM was performed to ensure higher surface tension/lower hygroscopicity of the wood.

2.1. Wood particle preparation

Beechwood originates from Slovenian forests. No growth anomalies were present, and there was no sign of fungal infestation that could affect the results. Kiln-dried beech (*Fagus sylvatica*) boards were collected and cut into smaller lamellas (900 mm × 200 mm × 25 mm). They were dried to an absolute dry state for 24 h at (103±2) °C and weighed to calculate the mass loss during the subsequent TM, which was performed in a vacuum modification chamber (Kambič d.o.o., Semič, Slovenija) according to the Silvapro method in semi-anoxic conditions (Pohleven and Rep 2001). The process of TM was divided into the following three stages: temperature increase (heating), modification process (constant temperature 180 °C/200 °C for 3 h) and temperature decrease and conditioning (cooling).

After TM, the wood boards were reweighed to determine mass loss during modification and cut into small cubes (20 mm × 20 mm × 20 mm). The cubes were also cut from non-thermally modified beech wood boards. All cubes were ground in a laboratory cutting mill SM 2000 (Retsch, Haan, Germany) first with a 1 mm sieve and in a second step with a 0.25 mm sieve. The obtained wood particles were then sieved through a 237 µm sieve and stored in airtight containers for further processing.

2.2. Compounding

The filament was produced in a two-step process to ensure better homogeneity. In the first step, the wood was mixed with a polymer matrix to form pellets, which were extruded into filaments in the second step.

Prior to compounding, wood flour was dried at 103 °C for 24 h and PLA granules at 60 °C for 12 h. After drying, the components were compounded using a laboratory-scale Brabender twin-screw extruder (Brabender, Duisburg, Germany) with a screw diameter of 20 mm and a length of 40D. The compounding process was carried out in the laboratory, and gravimetric feeders were used. Extruding temperatures were 210-190-180-190 °C, respectively, from hopper to die.

For pelletising, the EUP50 underwater pelletising system (Econ, Weisskirchen, Austria) was used. The pellets were dried at 60 °C for 12 h before further processing.

2.3. Filament extrusion

A Brabender KDSE Mark II extruder (Brabender, Duisburg, Germany) with a round section die 1.8 mm × 28 mm was used for filament extrusion. The pre-dried compound material had a moisture content of less than 0.1%. The extrusion temperatures were 220-210-175 °C, respectively, from the hopper to the die. A water bath at 70 °C or a conveyor belt with air cooling was used in the cooling phase.

The quality was ensured with a standard filament diameter using Accuscan 5012 (Beta LaserMike, High Wycombe, United Kingdom) for the desired diameter of 1.75 mm ± 0.05. The haul-off unit had a defined force, and speed synchronised with an automated winding unit. Approximately 200 m of each filament (different wood ratio, type of wood used) was produced, as listed in Table 1.

2.4. Fused filament fabrication of 3D-printed parts

All specimens were modelled in SolidWorks software (SolidWorks Corp., Waltham, MA, USA) and exported in the STL

Table 1. List of formulations (components mass ratios) and marking of prepared filaments.

Formulation code	PLA (wt%)	Beech (wt%)	TM beech at 180 °C (wt%)	TM beech at 200 °C (wt%)
PLA	100			
B10	90	10		
B20	80	20		
TM_180_10	90		10	
TM_180_20	80		20	
TM_180_30	70		30	
TM_200_10	90			10
TM_200_20	80			20
TM_200_30	70			30

format. The STL models were sliced and prepared for 3D printing using Cura software (Ultimaker, Utrecht, Netherlands). Specimens were printed using a Creality CR10-V3 3D printer (Creality 3D Technology Co., Ltd., Shenzhen, China) with a direct extruder. The nozzle diameter was 1 mm, the print layer thickness was set to 0.5 mm, the printing temperature to 220 °C, and the bed temperature to 50 °C. The specimens were printed with solid layers, with printing lines alternating at an angle of 45° (one layer +45°, next layer –45°) to the specimens' length.

Specimens 3D-printed for tests (Figure 1):

- dim. 120 mm × 15 mm × 4 mm (A) – used for dimensional stability and bending tests,
- dim. 50 mm × 50 mm × 10 mm (B) – used for density, water contact angle, surface roughness and indentation hardness measurements,
- dim. 46 mm × 10 mm × 4 mm (C) – used for rheometry,
- dog-bone shapes (type 1BA - 75 mm length), according to the standard EN ISO 527-2: 1996 (D) – used for tensile tests,
- dim. 80 mm × 10 mm × 4 mm, according to standard EN ISO 178:2003 (E) – used for dynamic mechanical analysis.

2.5. Characterisation of wood-PLA filament and 3D-printed specimens

2.5.1. Density

The density of specimens was calculated from measured dimensions (digital calliper) and mass (balance).

The density (EN 323: 1993) of 3D-printed specimens was determined on 3D-printed specimens dim. 50 mm × 50 mm × 10 mm, 5 samples for each material variation and average values were determined.

2.5.2. Hygroscopicity and dimensional stability

The dimensional stability tests were performed in the TLS-01 laboratory drying tunnel (Kambič, Semič, Slovenia). The dimensions of these specimens were 120 mm × 15 mm × 4 mm (length × width × thickness). In the test chamber of the drying tunnel, with dimensions 700 mm × 400 mm × 610 mm (length × height × width), humidification and drying processes were controlled by DPC-420 central microprocessor controller (Kambič, Semič, Slovenia). Air temperature (T), relative humidity (RH), and air velocity (v) ($\Delta T = \pm 1.0$ °C, $\Delta RH = \pm 1.0\%$, $\Delta v = \pm 0.1$ m × s^{-1}) were adjusted accordingly.

After 3D printing, specimens were conditioned in a climate chamber at 20% RH. To measure adsorption and desorption kinetics, samples (n = 7) were first exposed to 80% RH (humid climate) for seven days and then to 20% RH (dry climate) for the next seven days. The T was a constant 20 °C, and the air v was 1 m × s^{-1}. The sorption process of the 3D-printed samples was monitored by interval weighing of each sample on an Exacta 300 EB laboratory balance (Tehtnica, Železniki, Slovenia; m = ± 0.1 g) and by manual measurement of the three dimensions with a digital calliper (d = ± 0.01 mm).

The protocol and calculations were adjusted according to our recent research (Krapež Tomec *et al.* 2021).

The change in moisture content and, consequently, the dimensional stability and shape change of 3D-printed swelling polymers can be considered similar to solid wood under transient conditions by the system's response to an instantaneous, constant external perturbation. This is characterised by the transition of the system to a new steady state, which can be described as a first-order system (FOS) with a differential equation. From it, the response of the sample can be derived and determined by observing the change in mass and the resulting expansion or contraction of the samples and calculating the time constant (τ-tau) using Equation (1) (Bučar 2007, Straže 2010):

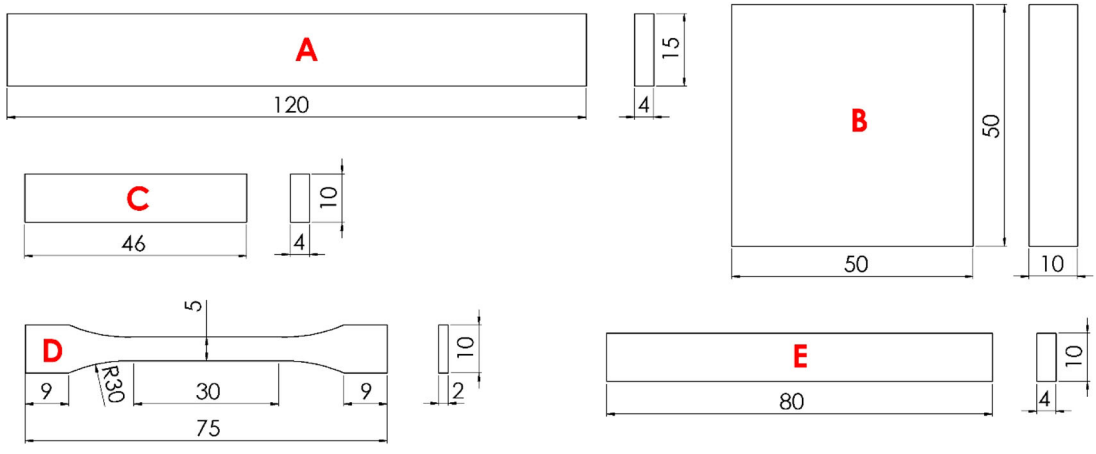

Figure 1. 3D-printed specimens for tests and their dimensions (A- used for dimensional stability and bending tests, B for density, water contact angle, surface roughness and indentation hardness measurements, C for rheometry, D- for tensile tests, E for dynamic mechanical analysis).

$$G\Phi(t) = \tau\frac{dm}{dt} + m \quad (1)$$

G – stationary system response in g, Φ (t) – transient system response, τ – time constant in s, m – mass in g, t – time in s.

The initial mass of the sample (m_i), the mass of the sample at a specific time (m_t), and the final or equilibrium mass (m_f) are introduced in the above equation to be equivalent to the stationary response (G), which is reached after a sufficiently long conditioning time.

The above equation for the case of instantaneous loading at time t = 0, with the initial condition m = m_i, can be then written in the following form:

$$m_t = m_f + (m_i - m_f) * e^{-\frac{t}{\tau}} \quad (2)$$

By transforming the expression (Equation (2)), the dependence of the average dimensionless mass change, i.e. the moisture ratio (MR), can be obtained as follows (Equation (3)):

$$MR = \frac{m_t - m_f}{m_i - m_f} = e^{-\frac{t}{\tau}} \quad (3)$$

The variable (m_t) reaches 63.2% of the instantaneous load G when the condition t = τ is reached. The final response of the system (99.9%) is usually reached after 5τ (Bučar 2007, Straže 2010). By monitoring the mass of the samples, we calculate the time constant by logarithmising the expression (Equation (4)):

$$\tau = \frac{t}{\ln\left(\frac{m_t - m_f}{m_i - m_f}\right)} \quad (4)$$

2.5.3. Modulus of elasticity (MOE)

The modulus of elasticity (MOE) of 3D-printed specimens of selected materials was determined on specimens used to determine dimensional stability (Section 2.5.2). MOE was tested after conditioning in two climates with different RH (20% and 80%) at 20 °C for 240 h.

The specimens were tested in a three-point bending test on the Z005 universal testing machine (ZwickRoell GmbH, Ulm, Germany). The support span L_s was 80 mm, and the loading rate was 10 mm × min^{-1}. To determine MOE, the specimens were loaded to about 30% of the maximum loading force (for each material, one specimen was loaded to failure), and MOE was determined accordingly:

$$MOE = \frac{L_s^3\,(F_2 - F_1)}{4bt\,(U_2 - U_1)} \quad (5)$$

L_S is the distance between supports, b and t are the width and thickness of the specimen, respectively, (F_2–F_1) is the increment of the load on the straight line of the load-deflection curve, (U_2–U_1) is the increment of deflection corresponding to (F_2–F_1).

The values given for each material were calculated as the average values of seven specimens for each RH/climate.

2.5.4. Indentation hardness

The hardness of 3D-printed specimens was measured using an instrumented indentation tester Step 300 (Anton Paar, Graz, Austria). On specimens (dim. 50 mm × 50 mm × 10 mm), nine measurements were performed for each variant. The linear loading protocol was used, with a maximum load of 25 N, a loading rate of 25 N × min^{-1}, and an unloading rate of 25 N × min^{-1}. The acquisition rate was 50 Hz.

The indentation hardness (H_{IT}) was calculated as the maximum load (F_{max}) on the projected area of the hardness impression (A_p), and the indentation modulus (E_{IT}) was calculated from the plane strain modulus (E*) using an estimated Poisson's ratio (ν) of 0.3, of the specimens:

$$H_{IT} = \frac{F_{max}}{A_p} \quad (6)$$

$$E_{IT} = E^* \cdot (1 - \nu_s^2) \quad (7)$$

2.5.5. Tensile strength

The tensile tests were made on 3D-printed specimens (for evaluation of 3D-printed product properties). Dog-bone shapes (type 1BA – 75 mm length), according to the standard EN ISO 527-2: 1996 (Plastics – Determination of tensile properties) were used. A test speed of 5 N × min^{-1} was used. Ten 3D-printed specimens were tested for each combination of materials using a Z005 universal testing machine (Zwick-Roel, Ulm, Germany), from which average values were determined. All tests were conducted at the T 23 ± 2 °C and RH 50 ± 10% on a minimum of 10 specimens, according to the standard EN ISO 527-2:1996.

2.5.6. Water contact angle measurements

Contact angle (CA) has been used as an indicator of the wettability of 3D-printed parts. An optical tensiometer Theta (Biolin Scientific Oy, Espoo, Finland) was used to determine the CA of water using the sessile drop method. Droplets with a volume of 4 µl of distilled water were dispensed. The CAs of the water droplets were determined after a transition time of 5 s after their application on the specimen's surface, following the established protocol of Nussbaum (1999). Five water droplets were analysed for each variant.

2.5.7. Surface roughness of the filaments and 3D-printed parts

A Lext OLS 5000 (Olympus, Tokyo, Japan) confocal laser scanning microscope (CLSM) was used to evaluate the surface roughness of the filaments and of the 3D-printed parts (average surface roughness parameter *Sa*). The surface roughness parameter (Sa) is commonly used to evaluate surface roughness and is defined as the arithmetic mean of the absolute ordinate values within a given range. Five spots with an area of 40 µm² were examined on each sample using a 20× magnification objective.

2.5.8. Rheometry

All measurements of rheological properties were performed using an ARES G2 rheometer (TA Instruments, New Castle, DE, USA) and Trios software (TA Instruments, New Castle, DE, USA). Parameters were the same for all specimens, dimensions 46 mm × 10 mm × 4 mm, rectangular torsion fixture was used. A strain sweep and a temperature ramp test were made to

evaluate the effect of the material on the properties of the 3D-printed specimens. Nine different printing materials were tested (PLA, B10, B20, TM180_10, TM180_20, TM180_30, TM200_10, TM200_20, TM200_30).

The amplitude sweep measurement measures the response of a material to a changing amplitude. It shows where the elastic modulus (storage modulus) is approximately the same (linear range), and it also shows where the nonlinear region begins. Oscillatory tests with a constant frequency of 1 Hz and variable amplitude were made.

The rheometer stopped measuring when the rheometer maximum load was reached, which was always in the nonlinear region of the specimen. From these measurements, the maximum elastic modulus (storage modulus) and the limit of the linear viscoelastic region (LVR limit) were determined. The amplitude (strain) at which the elastic modulus drops by 5% was determined as the limit of the LVR.

The temperature sweep test shows the response of the material to changing temperatures. The specimen was subjected to an oscillating torsional load with an amplitude (strain) of 0.4% at 1 Hz as the temperature increased from 25 °C to 130 °C.

The response of the elastic modulus (storage modulus) to the heating of the material was observed, and the glass transition temperature was determined using the tan δ curve. Tan δ is the ratio between the viscous modulus (loss modulus) and the elastic modulus (storage modulus). The peak of the tan δ curve indicates the glass transition temperature.

The glass transition temperature (T_g) is a transition state during the heating or cooling of amorphous materials. Long polymer chains are randomly oriented and move more freely when the glass transition temperature is reached. The glass transition temperature is always lower than the melting temperature (Petrič 2008). Our assumption was that rheological properties (elastic modulus) decrease with increasing wood content in the printing material.

2.5.9. Dynamic mechanical analysis (DMA)

DMA can provide important information about the compatibility of wood and other polymers. The DMA (ElectroForce 3300, TA instruments, New Castle, Delaware, USA) was used to determine viscoelastic properties at a fixed temperature. A sinusoidally varying strain was applied to the specimens in a 3-point bending clamp; the measurements were made at a constant temperature of 22 °C and at a varying frequency from 1 to 100 Hz. The specimens were rectangular and had dimensions of 80 mm × 10 mm × 4 mm according to EN ISO 178:2003, with printing lines at an alternating angle of 45° (one layer +45°, next layer −45°) to the specimen length. Nine different material compositions were used. The tests were performed using a 3-point bending clamp with a 60 mm span. At least 5 specimens of each type were tested at this stage, and their average was calculated.

The results of the measurements help to evaluate the influence of the wood content in the composite and the printing conditions on the properties of the printed parts.

2.5.10. Scanning electron microscopy (SEM)

A Quanta 250 scanning electron microscope (Thermo Fisher Scientific, Waltham, MA, USA) was used to visually assess the microstructure between different materials (wood particle additions) and to evaluate the dispersion of the wood particles in the PLA matrix. The filaments were cross-sectioned and smoothened on a sledge microtome SM2010R (Leica Microsystems GmbH, Wetzlar, Germany). The analysed surfaces were sprayed with a conductive gold layer prior to SEM observations. Images of the area on the surface of the specimens were acquired at three different magnifications (80×, 100×, 500×) in high vacuum (1.56×10^{-2} Pa) with an electron source voltage of 5.0 kV.

2.5.11. Statistics

Statistical analysis of data was performed using Microsoft Excel (Microsoft, 2019, Redmond, WA, USA) and GraphPad Prism (GraphPad Software, 9.0, San Diego, CA, USA). The statistical significance of measured differences was analysed with basic statistical analysis, and the results were checked for analysis of variance (ANOVA).

3. Results

3.1. Density

The density of raw materials for the production of filament PLA 1240 kg/m^3, the density of beech wood (B) (623 kg/m^3) and TMd beech wood (TM180 – 615 kg/m^3 and TM200 – 602 kg/m^3) was calculated from absolute dry wood specimens (mass divided by volume). Higher modification temperatures resulted in higher mass losses of beech wood during modification. Namely, the mass loss during thermal modification was 2.31% (TM 180 °C) or 6.50% (TM 200 °C). The mass loss of TMd specimens was calculated using the absolute dry wood specimens before and after TM from an average of 16 specimens. Mass loss of thermally modified wood is in line with reference data (Rep *et al*. 2012, Humar *et al*. 2020). The density of 3D-printed specimens is presented in Figure 2.

The density of printed composite samples depends on the density of raw materials, density of filaments (possible voids in filaments cross-section), printing settings (infill percentage, flow settings, etc.) and anomalies that occur during printing

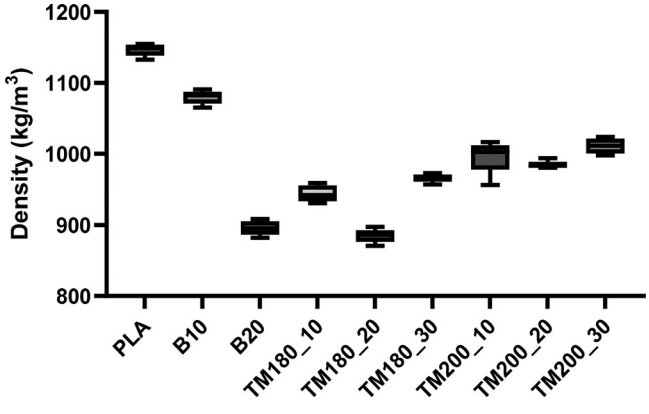

Figure 2. Density of 3D-printed specimens.

(nozzle clogging, uneven material flow, formation of gasses at higher extrusion temperature, moisture in filament, etc.). Specimens printed from wood PLA filament with 20% TM180 had the lowest density (885 kg/m^3), specimens from filament with 20% beech wood had a similar value (896 kg/m^3), while specimens with 20% TM200 wood had a density, that is 11% higher than previously mentioned specimens (985 kg/m^3). This phenomenon might be the result of lower void content/lower porosity in TM200 specimens. The density of the specimens printed from pure PLA filament had the highest value (1146 kg/m^3), which is slightly lower than the density of PLA used 1240 kg/m^3 (TDS 2019), followed by 10% unmodified beech wood specimens (1080 kg/m^3) and 30% TM200 specimens. The density of beech wood is lower than the density of PLA, so the addition of wood could reduce the density of 3D-printed parts. This hypothesis was confirmed in most cases, except for specimens with a 30% addition of TM wood. This could be due to better encapsulation of the wood particles with PLA and lower void content. One of the possible reasons for the higher density of PLA composites made in combination with TM200 could be the size of the wood. Wood modified at higher temperatures is more brittle; thus, the wood particles might be smaller and of more even shapes than the ones made of TM180 and non-modified wood.

The difference between theoretical (calculated from raw material densities and ratios in composites) and measured density was calculated, taking into account PLA/wood proportion for each combination of composites. We assume that the difference corresponds to the percentage of voids in printed parts (Table 2), which were caused either by material causes (voids in filament, surface roughness of filament, gasses formation, moisture evaporation) or printing process causes (raster gap voids, partial neck growth voids, sub perimeter voids (Tao *et al*. 2021)).

The percentage of voids is assumed to be the lowest in TM200_30, as there seems to be the best interlayer compatibility.

A lot of factors influence the formation of voids, from particle sizes and distribution of particle sizes, compatibility of wood and polymers, and the 'encapsulation' of particles with polymer. Different voids are seen on microscopic images of filaments and 3D-printed parts. The presence of any kind of voids is unwanted from the view of mechanical properties since they could act as stress concentrators and start failures during loading (van de Werken *et al*. 2020).

3.2. Hygroscopicity and dimensional stability

The reason for using TMd wood, in addition to better compatibility with PLA, is expected lower water absorption and thus higher dimensional stability of the TMd wood and thus of the composite. The ground particles of TMd wood are smaller due to their fragility, affecting the filament's better flowability during extrusion through the printing nozzle, thus eliminating one of the main problems in 3D printing with wood-plastic composites.

The results show that the dimensional stability of 3D-printed parts depends on the material used (Table 3). The lowest longitudinal swelling was observed in specimens made of pure PLA; it was 0.05% when exposed to a dry to humid climate (between 20% and 80% RH). Specimens made of wood-PLA exhibited higher longitudinal expansion (0.14% and 0.28%). Moisture adsorption increases with wood content in composites due to the free hydroxyl groups (-OH) of hemicelluloses and amorphous cellulose in the cell walls of wood fibres (Cristian Neagu *et al*. 2006). Therefore, wood-plastic composites with higher wood content adsorb more moisture when exposed to higher humidity (Table 3). Although TM reduces the hydrophilicity of wood, this was not evident in the results of final mass gain, length expansion and differential swelling. Differences in moisture content after humidification were not significant among the investigated specimens of B10 and TM200_10 (ANOVA, $p = 0.423$). The reason could be in particle sizes and particle size distribution. TMd wood particles were smaller and with a higher ratio of smaller particles (Krapež Tomec *et al*. 2023) and thus had higher specific particle surface, and polymer could not fully cover all the wood surface, and moisture had more access to wooden material. As noted with wood-plastic composites (WPC), the particle size of the wood affects water absorption, and as this ratio increases, so does water absorption (Križan *et al*. 2020). It was also found that an intact composite surface corresponds to a lower moisture transport rate within the polymer matrix (Segerholm *et al*. 2012). The reduced hygroscopicity of TM wood is caused by cleavage of hydroxyl groups and also softening and cross-linking of lignin reducing the number and availability of sorption sites. The MC can thus, be drastically reduced with thermal modification, sometimes up to 50% (Hill 2006). Nevertheless, thermal modification often improves the dimensional stability and resistance to decay of wood. These enhancements

Table 2. Void content – assumption as the difference between calculated/theoretical and measured density of 3D-printed specimens.

Specimens	Measured density (kg/m^3)	Calculated density* (kg/m^3)	Calculated void content (%)
PLA	1146	1240	7.5
B10	1080	1178	8.4
B20	896	1117	19.8
TM180_10	944	1178	19.9
TM180_20	885	1115	20.6
TM180_30	966	1053	8.2
TM200_10	997	1176	15.3
TM200_20	985	1112	11.5
TM200_30	1011	1049	3.6

* Based on raw material densities and ratios in composite

Table 3. Mean weight gain, length expansion, differential swelling (length expansion per % of moisture change) and moisture content (MC)* of tested specimens after humidification cycle.

Specimen	Final mass gain (%)	Length expansion (%)	Differential swelling (%)	Moisture content (%)
PLA	0.41	0.05	0.0009	0.63 ± 0.03
B10	0.65	0.14	0.0024	1.05 ± 0.04
B20	1.48	0.28	0.0046	2.12 ± 0.05
TM180_10	0.83	0.18	0.0029	1.21 ± 0.05
TM180_20	1.39	0.23	0.0038	1.98 ± 0.03
TM180_30	1.83	0.26	0.0043	2.61 ± 0.04
TM200_10	0.76	0.23	0.0039	1.09 ± 0.01
TM200_20	1.18	0.27	0.0045	1.73 ± 0.03
TM200_30	1.58	0.28	0.0046	2.26 ± 0.04

* Results are expressed as the mean value of measurements with standard deviations.

Table 4. Dynamics of weight change and length change of tested materials determined by time constant τ (tau) in First Order System.

	Tau from mass (h)		Tau from length (h)	
	humidification	drying	humidification	drying
PLA	34.48	13.51	24.39	52.63
B10	47.62	45.45	52.63	55.56
B20	30.30	21.74	55.56	40.00
TM180_10	47.62	43.48	55.56	71.43
TM180_20	26.32	26.32	50.00	41.67
TM180_30	43.48	35.71	45.45	43.48
TM200_10	30.30	22.73	41.67	31.25
TM200_20	47.62	35.71	27.78	50.00
TM200_30	50.00	32.26	26.32	47.62

can contribute to the long-term durability of the wood-polymer composite, affecting the integrity of the bonding over time. Also, when the hygroscopicity of the wood is decreased by TM, the WPCs can be used in more severe conditions (Ayrilmis *et al*. 2011).

In Tukey's multiple comparison test, the differences between all investigated specimens, except B10 vs. TM200_10, were significant (ANOVA, p <0.0001).

The dynamics of mass and length change of nine different materials, determined by the time constant τ (tau) in the first-order system, are shown in Table 4. The dynamics of moisture adsorption from mass are, for most materials, slower than the dynamics of drying.

Our hypothesis was that specimens with a higher wood content (20%, 30%) would take longer to reach mass equilibrium due to their greater moisture adsorption capacity, which did not prove to be true. Another assumption was that materials with the addition of TMd wood would have lower tau and shorter equilibrium time, which was partially true for specimens from filament with wood TMd at 200 °C.

3.3. Tensile strength of 3D-printed parts

Tensile strength (Figure 3) was highest for specimens made of pure PLA (50 MPa), followed by specimens with a 10% addition of wood (B10, TM180_10, TM200_10). Specimens with a 30% addition of TM wood (TM180 or TM200) have the same tensile strength as specimens made of filament with 20% unmodified beech wood (27 MPa).

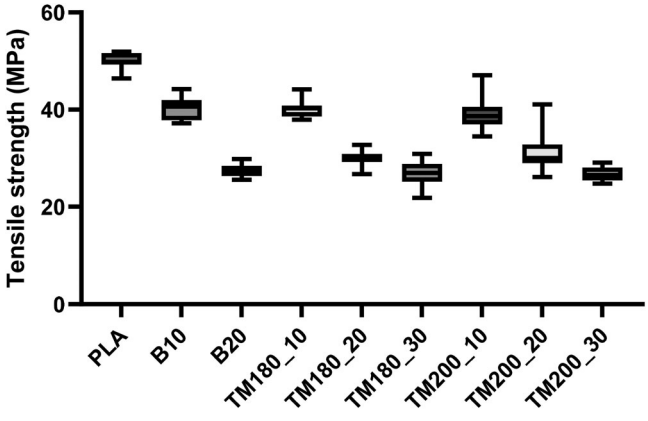

Figure 3. Tensile strength of 3D-printed specimens from PLA filament, filaments with added beech wood (B10, B20) and thermally modified beech wood (TM180_10, TM180_20, TM180_30, TM200_10, TM200_20, TM200_30).

Previous research has shown that tensile strength values decrease with higher proportions of wood particles. At low wood content, the wood particles can act as reinforcement, but at higher loading levels, the polymer cannot fully enclose the particles, resulting in poor bonding and limited load transfer. The wood particles used in this study had a relatively small aspect (length vs. cross-section) ratio and could not contribute to the mechanical properties to the extent that longer fibres/particles would. Lower tensile strength in parts with higher wood content is probably also due to the void content within the filament and between printing layers in the specimens, as well as to poor interfacial bonding between matrix and filler.

There is no evident effect of TM on tensile strength, as specimens with TM wood particles have almost the same strength as parts with unmodified wood. It is not possible to determine whether the better compatibility of TMd wood and polymer and the smaller particles of TMd wood affect the strength reciprocally or mutually.

Kariž *et al*. (2018) reported that small proportions of wood powder (10% and 20%) in wood-PLA filaments resulted in higher tensile strength (57 MPa) of the filaments, while larger proportions of wood powder (50%) resulted in lower tensile strength (30 MPa) of the filaments.

3.4. MOE in bending test

In contrast to the trend in tensile strength, the modulus of elasticity (Table 5) tended to increase with increasing wood content, except for specimens with 20% wood addition. This could be related to the lower density of the aforementioned specimens. The highest MOE were obtained for the samples TM200_30 (3886 N/mm^2) at 20% RH. Differences in modulus of elasticity were not significant among the investigated specimens (ANOVA, $p = 0.201$ for MoE at RH 20% and $p = 0.799$ for MoE at RH 80%).

The mechanical properties of wood-plastic composites also depend on the moisture content (MC) of the material. Higher stiffness was observed after conditioning the specimens in a drier climate (20 °C and 20% RH). The results may reflect the findings of solid wood, where the mechanical properties (including the MOE) tend to be below the MC of saturation of the primary sorption sites (Martikka *et al*. 2018). The composites with a higher percentage of wood particles and larger particles (B10, B20) also absorb more water, which causes a weaker bond between the polymer (nonpolar) and wood (hydrophilic) (Humar *et al*. 2020, Hill *et al*. 2021). With TM, wood becomes

Table 5. Mean modulus of elasticity (MOE) with standard deviation and moisture content (MC) for specimens conditioned at 20 °C and 20% or 80% RH.

	20% RH		80% RH	
	MOE (N/mm^2)	MC (%)	MOE (N/mm^2)	MC (%)
PLA	3670 ± 226	0.22	3337 ± 166	0.62
B10	3758 ± 162	0.97	3477 ± 119	1.05
B20	2501 ± 52	0.63	2293 ± 40	2.12
TM180_10	2734 ± 104	0.38	2580 ± 108	1.21
TM180_20	2413 ± 119	0.59	2234 ± 182	1.98
TM180_30	3399 ± 158	0.76	3042 ± 135	2.61
TM200_10	3431 ± 168	0.33	3268 ± 257	1.09
TM200_20	2771 ± 510	0.54	2587 ± 480	1.73
TM200_30	3886 ± 252	0.67	3395 ± 163	2.26

more hydrophobic and thus more similar to the polymer, which also makes their bond stronger and MOE higher.

Wood-plastic composites retain some of the properties of wood, such as absorption of water under humid conditions. This absorption is limited by polymer enveloping the particles and preventing the direct contact of moisture with wood parts. TM of wood lowers its equilibrium moisture content (EMC), and it slows down water vapour sorption. In a recent study, Majka and co-authors (Majka *et al*. 2022) found that the EMC of untreated beech wood particles (size 0.80-0.250 mm) was 0.21 kg/kg and of TMd beech wood particles of the same size range was 0.19 kg/kg. However, our results show that printed parts with untreated beech wood have a lower moisture content. The reason could be the particle size and porosity- filaments with TM wood have smaller wood particles, and thus, the polymers cannot completely envelop all particles, and the water/moisture can penetrate deeper into the material.

The results were expected and are in line with previous reports (Kariz *et al*. 2018; Martikka *et al*. 2018, Ayrilmis *et al*. 2019, Kain *et al*. 2020, Krapež Tomec *et al*. 2021).

3.5. Wettability with water

Understanding the interactions between water and composites was achieved by measuring the static water CAs on the surfaces of the 3D-printed specimens (Figure 4). The water CA was the lowest for pure PLA specimens (69.7°), followed by specimen B20 (77.5°). Previous studies reported that the water contact angle values for PLA varied from 60° to 85° (Galindo and Ureña-Núñez 2018, Ayrilmis *et al*. 2019). CA was smaller on specimens with the addition of non-treated wood compared to specimens with the addition of TM wood. It was highest (91.7°) for specimens composed of 30% TM200, indicating greater hydrophobicity of TM wood. In addition, CA is influenced by surface roughness and porosity. Pores in the printed filaments can act as capillaries that absorb water (Petrič and Oven 2015). After 60 s, CA was 2–3° smaller due to the low penetration of water into the surface of the 3D-printed part.

For WPCs, the CA increases with higher polymer content (Lazrak *et al*. 2019). This trend was not evident in the 3D-printed specimens, especially in the TM200 specimens. In a previous study by Ayrilmis *et al*. (2019), the 1 s CA of water on the specimens increased from 67.8° to 97.3° when the wood flour content was elevated from 10 to 40 wt%.

The CA values on the 3D-printed wood-PLA specimens with wood content up to 30 wt% were below 90°, which favoured the wetting behaviour of all specimens. Nevertheless, the incorporation of wood particles into the PLA matrix significantly reduced the wettability of the specimens.

In contrast, our goal was to improve the interface between the wood particles and a polymer matrix. Hydrophilicity leads to water absorption and, once incorporated, to dimensional instability and, thus, to a deterioration of the mechanical properties of the composite. TM can thus work in favour of the hydrophobicity of the composite.

3.6. Surface roughness

The surface roughness of filaments and 3D-printed parts was evaluated using CLSM.

The surface roughness of filaments increased with wood content (Figure 5). As expected, filaments with TM wood have lower roughness than filaments with untreated wood particles at the same particle ratio in the composite due to the assumption of smaller TM particles and lower porosity. The porosity of 3D-printed products is directly related to the reduction of mechanical strength and increased water absorption and swelling rate (Ayrilmis *et al*. 2019).

The quality of the processed filament strongly influences the performance of printed parts. The geometry of the filament, inhomogeneities, and voids can be transferred into the 3D-printed part, resulting in poor part properties and performance (Unterweger *et al*. 2018). Therefore, the surface roughness of the 3D-printed specimens followed a similar trend to the filaments: it was lowest for pure PLA specimens and increased with a load of wood particles. All versions of TM wood had lower values than 20% beech wood (B20).

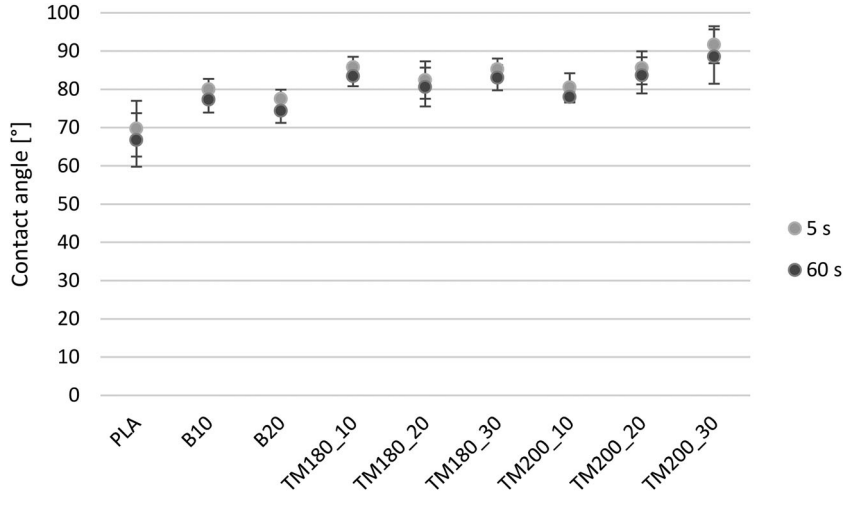

Figure 4. Contact angle on 3D-printed specimens from PLA filament, filaments with added beech wood (B10, B20) and thermally modified beech wood (TM180_10, TM180_20, TM180_30, TM200_10, TM200_20, TM200_30) after 5 and 60 s.

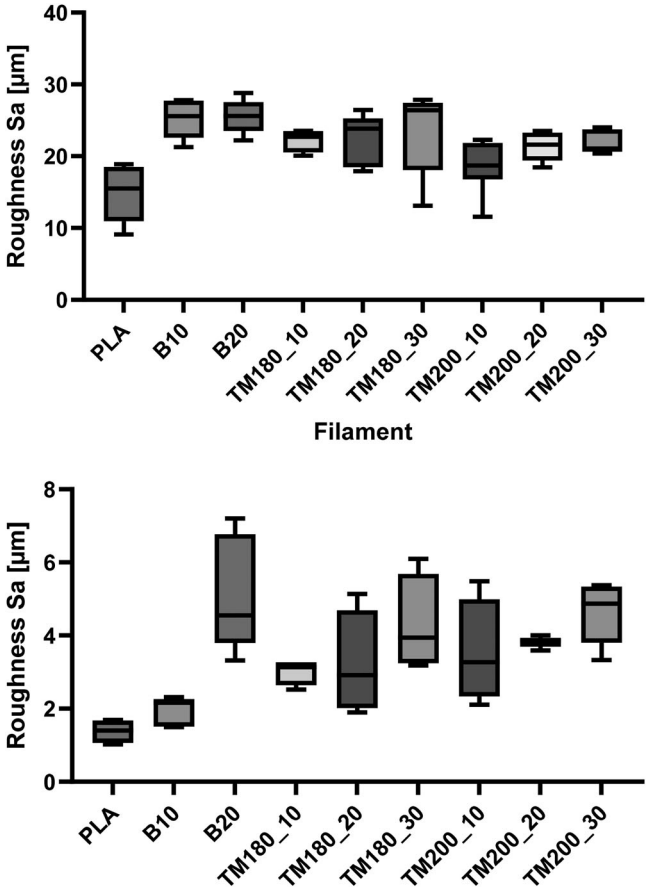

Figure 5. Surface roughness of filaments (top) and 3D-printed specimens (bottom) from PLA, filaments with added beech wood (B10, B20) and thermally modified beech wood (TM180_10, TM180_20, TM180_30, TM200_10, TM200_20, TM200_30).

3.7. Indentation hardness

The indentation hardness of 3D-printed specimens was measured using an instrumented indentation tester. The decrease in the hardness of the 3D-printed specimens was reflected in an increase in the depth of the indentations caused. A certified 6 mm diameter ball was used for the indentation in the specimen with the diagonal printing lines of 0.5 mm height.

The results show that the indentation hardness of 3D-printed specimens (Figure 6) is highest for specimens made of pure PLA (2445 MPa), followed by specimens from filament with 10% beech wood additive (1675 MPa), while specimens with the addition of TMd wood have lower values. In contrast to specimens with untreated beech wood addition, specimens with higher TM wood content (30%) exhibit higher indentation hardness than those with lower wood content.

The reason for the lower indentation hardness of the specimens with added TMd wood could be the lower hardness of TMd wood and its lower density compared to untreated wood.

Comparably, the indentation modulus of 3D-printed specimens (Figure 7) follows a similar trend.

Similar to MOE and the storage modulus, the indentation hardness and indentation modulus of specimens with TMd wood with the highest addition of wood (TM180_30 and TM200_30) are also the highest.

3.8. Rheology results

The storage modulus (G′) is the measure of the elastic behaviour of the specimen. An oscillating torsional load with an amplitude (strain) of 0.4% was induced while the temperature increased from 25 °C to 130 °C.

The G′ of the printed specimens from pure PLA filament was highest at 1.04 GPa. Previous studies found that pure PLA had a G′ value of 0.83 GPa (Kuzman *et al*. 2019), and solid beech wood had a value of 16.5 GPa (Kutnar *et al*. 2021). However, in our study, the addition of wood particles resulted in a decreased G′ (Figure 8).

The addition of 10% beech particles reduced G′ by 27%, and the addition of 20% wood by 38%. The PLA filament with the addition of 10% TM180 wood had the lowest value (0.63 GPa). Specimens with the addition of TM200 wood all had higher G′ values than specimens with the addition of untreated wood. We can conclude that at equal shape, fine

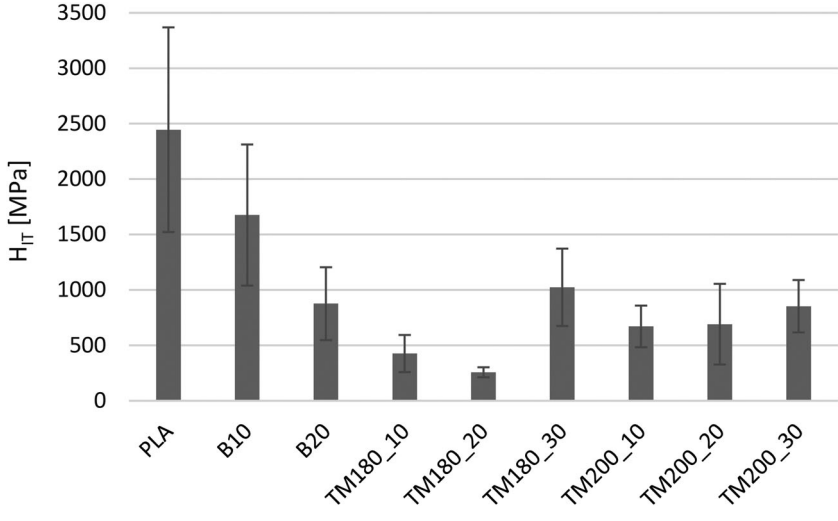

Figure 6. Indentation hardness of 3D-printed specimens from PLA, filaments with added beech wood (B10, B20) and thermally modified beech wood (TM180_10, TM180_20, TM180_30, TM200_10, TM200_20, TM200_30).

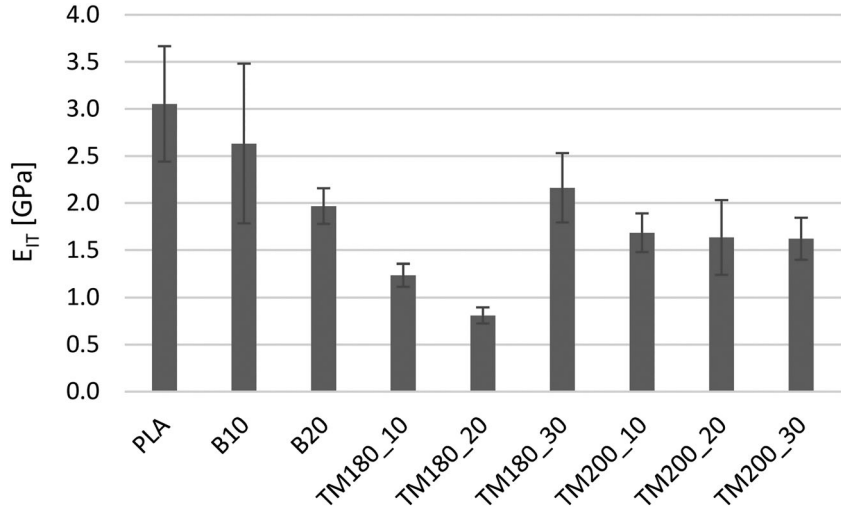

Figure 7. Indentation modulus of 3D-printed specimens from PLA, filaments with added beech wood (B10, B20) and thermally modified beech wood (TM180_10, TM180_20, TM180_30, TM200_10, TM200_20, TM200_30).

particles (of TM wood) have a greater surface area than coarse particles, and this favours the probability of more chemical bonding with the matrix (Mazzanti and Mollica 2020). The reason for the lower storage modulus could be due to clogging and clustering of the wood particles when the material is not fused. However, the addition of TMd wood resulted in an increase in G′ compared to specimens with untreated wood, especially at higher wood content levels. However, it has been previously reported that higher content of untreated wood in 3D-printed parts reduces the storage modulus measured with torsional loading on a rheometer (Kariz *et al*. 2018). In general, the modulus of elasticity indicates the ability of a material to deform under load, while the storage modulus measures the material's ability to store elastic energy. In some cases, there may be a positive correlation between MOE and max G′, indicating that a material with a higher modulus of elasticity also has a higher maximum storage modulus. This was also the case in our study. Similar to the MOE, the maximum G′ also rose when incorporating TMd wood particles and increased with higher wood content.

As discussed by Yue *et al*. (2022), wood powder, as a solid particle, cannot be melted and does not have the flow characteristics of a polymer melt. To some extent, it hinders the movement of the PLA molecular chain, increasing the melt viscosity of the composite and decreasing the flowability of the system. The interaction between the (modified) wood particles and the

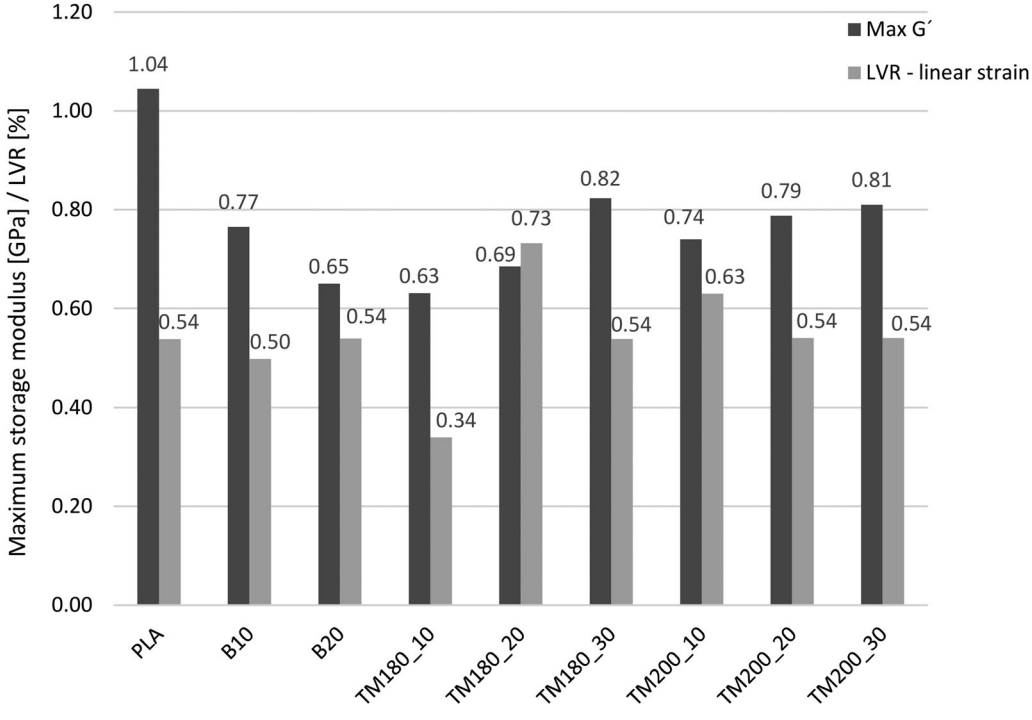

Figure 8. Maximum storage modulus and LVR of 3D-printed specimens from PLA, filaments with added beech wood (B10, B20) and thermally modified beech wood (TM180_10, TM180_20, TM180_30, TM200_10, TM200_20, TM200_30).

Table 6. The glass transition temperature of different filament compositions.

Filament	T_g (°C)
PLA	66.3
B10	64.9
B20	64.1
TM180_10	64.9
TM180_20	64.8
TM180_30	64.7
TM200_10	65.6
TM200_20	64.3
TM200_30	64.1

PLA matrix is the main element affecting the dispersion, rheological and mechanical properties (Yue *et al*. 2022). There were no significant differences between filaments in deformation at the LVR limit strain. The lowest deformation at the LVR limit strain was obtained for the filament with 10% TM180 wood content (0.34%) and the highest for the filament with 20% TM180 wood content (0.73%).

The highest and lowest LVR limit strain was found to be 0.996 and 0.315% for printed objects made from filaments with 20% and 50% wood flour content, respectively (Kariz *et al*. 2018).

The glass transition temperature was similar for all materials because the filaments had the same PLA base polymer (Table 6). Specimens made from pure PLA had the highest temperature (66.3 °C), while it was 0.7-2.2 °C lower for specimens made of wood-PLA filaments; the smaller wood phase has little effect on the material properties when heated. Specimens made from B20 and TM200_30 had the lowest glass transition temperature (64.1 °C).

In previous research by Ecker *et al*. (2019), the glass transition temperature of wood powder-based 3D-printed samples is lower than those of pure PLA, and the amount of wood content does not significantly affect the thermal properties (Tao *et al*. 2017, Ecker *et al*. 2019).

In contrast, a lower glass transition temperature usually means a lower melting temperature, which can help solidified layers fuse with the hot layers by effectively melting them together. Controlling melt rheology is the most practical way of reducing fibre breakage and achieving better filler distribution (Yan *et al*. 2013).

3.9. Results of dynamic mechanical analysis (DMA)

When combined with rheological and other analytical techniques, DMA can provide critical structure–property relationships linking material chemistry and microstructure to end-product performance characteristics (*TA Instruments*, n.d.). Since wood-polymer composites may be subjected to various dynamic stresses during their use, studies on the structures and viscoelastic behaviour of these materials are of great importance in determining their relevant stiffness and damping properties for various applications.

Compared to other mechanical tests, such as the tensile test, DMA operates mainly in the linear viscoelastic range and is, therefore, more sensitive to the chemistry and microstructure of the material. DMA measures viscoelastic properties with dynamic oscillatory tests.

Specimens made of filaments with 20% added beech wood (B20) were found to withstand lower frequencies and, therefore, last less time before breaking compared to specimens with the same addition of thermally modified beech wood (TM180_20, TM200_20). Furthermore, specimens with 20% and 30% TM200 wood added have a 13% and 33% longer test time, respectively, compared to the same TM180 wood addition.

The results of the 3D-printed specimens in the DMA frequency sweep test are consistent with the results of other mechanical tests in this study: higher additions of wood thermally modified at higher temperatures (TM200) demonstrate better mechanical properties (Figure 9).

The storage modulus measured with DMA at a frequency of 1 Hz using the frequency sweep method (Figure 10) has a similar trend to the maximum storage modulus measured with

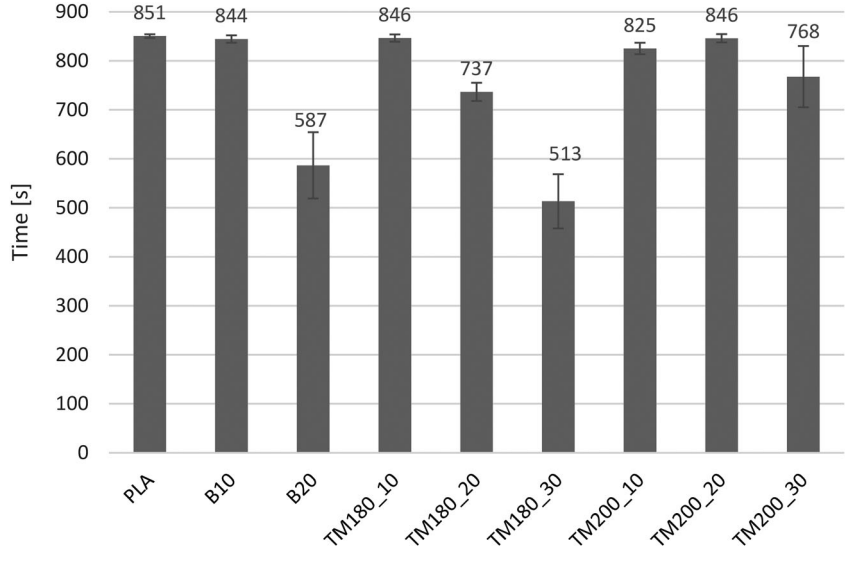

Figure 9. Frequency sweep test duration on 3D-printed specimens made of PLA, filaments with added beech wood (B10, B20) and thermally modified beech wood (TM180_10, TM180_20, TM180_30, TM200_10, TM200_20, TM200_30).

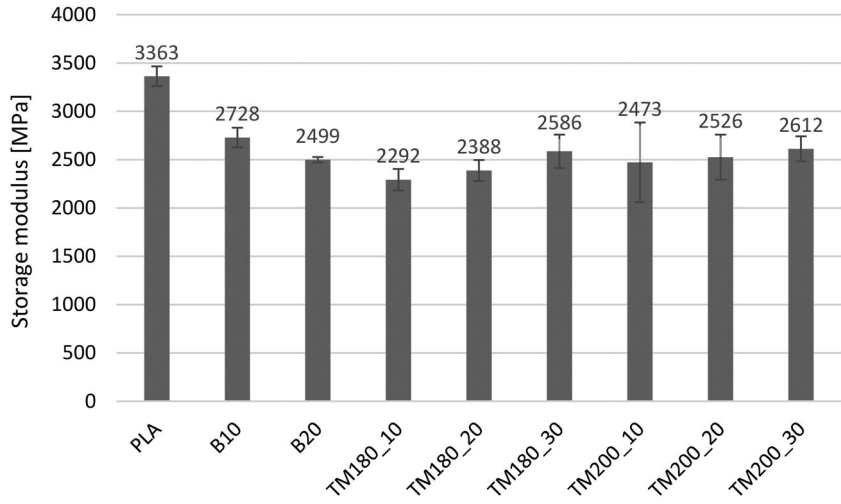

Figure 10. Storage modulus measured with DMA at a frequency of 1 Hz on 3D-printed specimens made of PLA, filaments with added beech wood (B10, B20) and thermally modified beech wood (TM180_10, TM180_20, TM180_30, TM200_10, TM200_20, TM200_30).

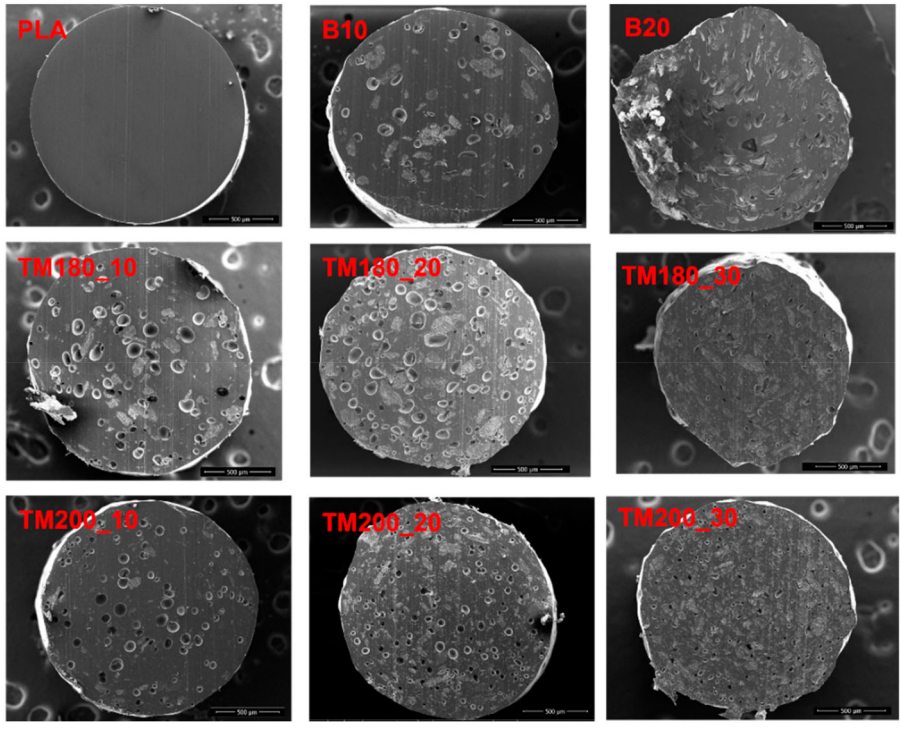

Figure 11. Cross-section of filaments from pure PLA, filaments with added beech wood (B10, B20) and thermally modified beech wood (TM180_10, TM180_20, TM180_30, TM200_10, TM200_20, TM200_30).

the rheometer using the amplitude sweep method (Figure 8). The highest storage modulus (3363 MPa) was found for specimens made of pure PLA, followed by specimens with a 10% addition of untreated beech wood (2728 MPa). Adding 20% beech wood particles reduced the storage modulus by 26%.

Comparable to the rheometer measurements, the lowest value (2292 MPa) for DMA PLA filament was obtained with a 10% addition of TM180 wood, and a higher storage modulus was obtained with the addition of TM200 than with the addition of TM180. In contrast to specimens with untreated wood, the storage modulus of specimens with TM wood increased with increasing wood content.

3.10. Scanning electron microscopy (SEM) images

The cross-section of nine filaments and 3D-printed specimens from these filaments were studied with SEM. Cross-sections of PLA filament with the addition of TM wood show smaller wood particles, which is due to the more brittle nature of TM wood. Filaments are more homogeneous and have smaller voids (Figure 11). In particular, filaments with TM at 200 °C exhibit a very round cross-section, lower porosity and good mixing of polymer and wood particles.

Electron micrographs show greater penetration of the polymer into the cells of the TM beech wood, suggesting

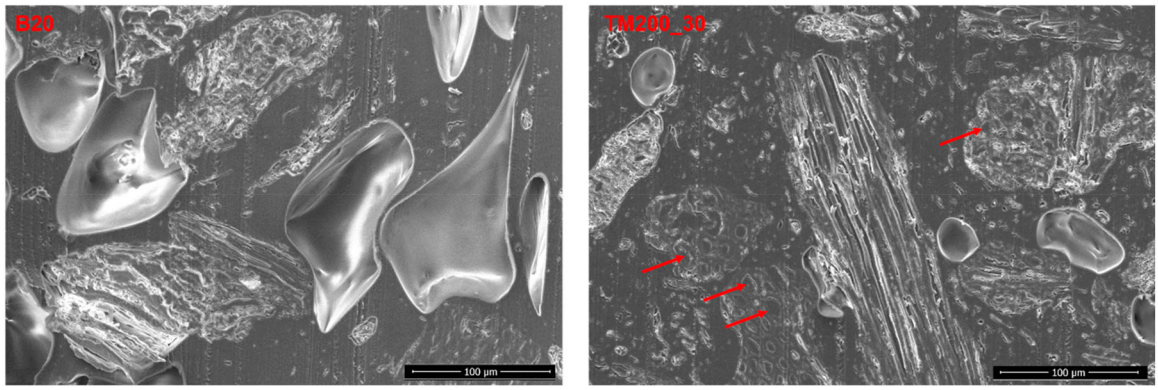

Figure 12. Cross-section of filament with 20% added beech wood (B20; left) and filament with 30% thermally modified beech wood (TM200_30; right); arrows indicating the penetration of polymers into wood cell lumens.

better compatibility of the modified wood with PLA (Figure 12). In the left figure (B20), process process-induced voids are very noticeable, while they are less evident in the right figure (TM20_30).

A similar trend in porosity and voids can be seen in the cross-section of 3D-printed parts. For specimens printed with pure PLA, the main voids are only the partial voids in the neck area and only a few very small voids within the extruded PLA strands. The addition of wood particles creates an additional number of voids in the extruded material. Some of these voids could be a tear out of the wood particles during the cross-section preparation, but mainly, these voids look like cut air bubbles in the material (smooth surface inside the voids). SEM micrographs of cross-sections of 3D-printed specimens with higher wood content show good interlayer compatibility (Figure 13).

Porosity is a common problem in FFF composites, especially fibre-reinforced polymer composites. In general, the term 'porosity' refers to voids caused by the manufacturing process that lead to a potential reduction in the mechanical properties of the final product, affecting its performance (Ezzaraa *et al*. 2023). Wang *et al*. (2019) reported that X-ray computed tomography and mechanical test results showed that the specimens with lower porosity had better mechanical properties. It is clear from the micrographs and the test results that higher porosity is closely associated with poorer mechanical properties. To some extent, the inferior mechanical properties of the 3D-printed wood-PLA composite are due to poorly bonded

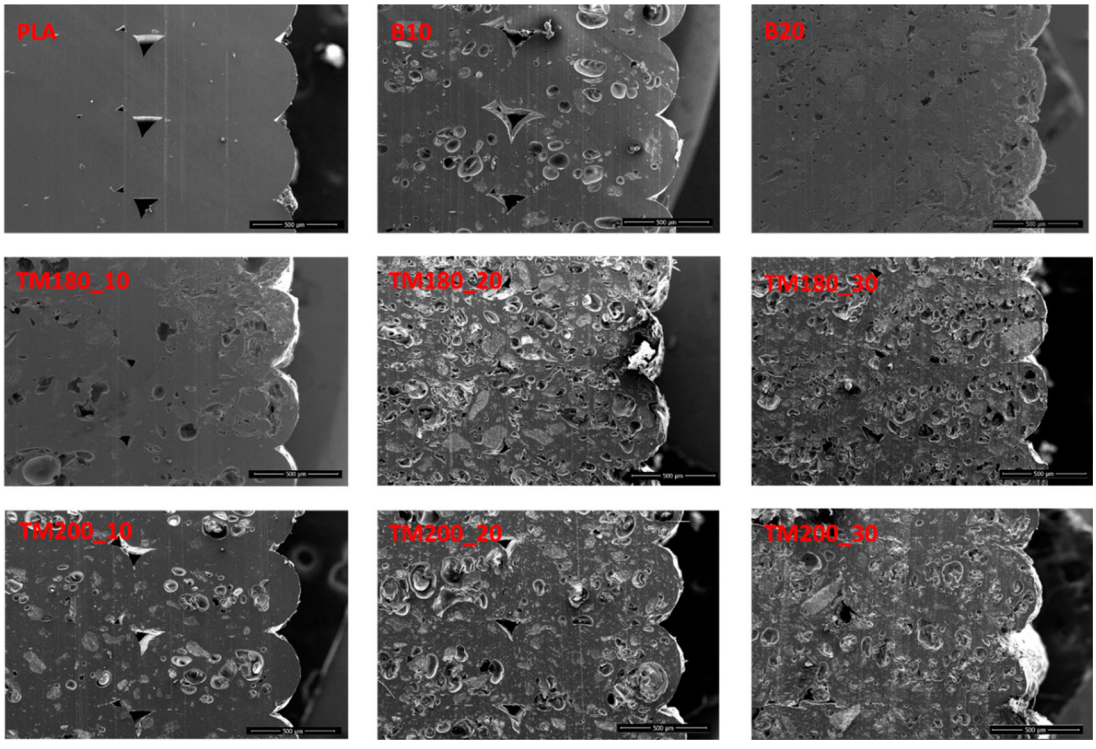

Figure 13. Cross-section of 3D-printed specimens; first row (from left to right): pure PLA, PLA with added beech wood (B10, B20); 2nd row: PLA with thermally modified beech wood at 180 °C (TM180_10, TM180_20, TM180_30) and 3rd row: PLA with thermally modified beech wood at 200 °C (TM200_10, TM200_20, TM200_30).

wood particles that transfer load ineffectively (Ezzaraa *et al*. 2022). This suggests that TMd wood is more strongly bonded to the polymer matrix since the TMd wood filaments' porosity is lower than the specimens from these filaments. In another study, Ayrilmis *et al*. (2019) reported that the porosity of 3D-printed wood-PLA specimens increased with increasing layer thickness. In the present study, the layer thickness was quite high (0.5 mm), so reducing the layer thickness would likely contribute to lower porosity and better mechanical properties of the specimens.

To sum up, thermal modification of wood causes altered surface chemistry, primarily from hemicellulose degradation, impacts compatibility and adhesion between wood particles and the polymer matrix. Changes in particle morphology (higher specific surface) and increased hydrophobicity of TMd particles further influence mechanical interlocking and interaction with the polymer, enhancing overall bonding and dispersion within the composite material.

4. Conclusion

The compatibility of the polymer and wood is important for an optimal end product/composite. TM makes the wood less polar and more hydrophobic, thus improving its compatibility with PLA.

Although we hypothesised that specimens with the addition of TMd wood would have lower weight gain and length expansion in moisture conditions, this could not be confirmed by the hygroscopicity test and dimensional stability tests. However, the addition of TMd wood results in quality improvement of the surface (lower roughness, higher water CA), higher maximum storage modulus, lower density of filament, and lower glass transition temperature. MOE and indentation hardness demonstrate the highest results by adding 30% TM wood. The general trend shows a decrease in tensile strength with increasing fibre content. However, the results from TM wood showed higher strength at the same filler content compared to unmodified wood. Several of these differences may be related to different particle sizes of the TM wood obtained by the same method of grinding as unmodified wood (Krapež Tomec *et al*. 2023).

Microscopic images suggest that TMd wood improves interfacial adhesion between particles and polymer, the void size is smaller, and the filler is more homogeneously distributed.

In addition, the parameter settings in the 3D printing process strongly influence the products' qualities and properties. Therefore, the optimisation process for composite production is crucial for producing high-quality products with improved properties. Since not much optimisation research has been done in the field of additive manufacturing of wood-polymer composites, this could be a gap to fill in the future.

Acknowledgements

The authors acknowledge the support of the Slovenian Research Agency (ARRS) within the framework of research programmes No. P4-0015 'Wood and lignocellulosic composites' and P4-0430 'Forest-wood value chain and climate change: transition to circular bioeconomy'.

Disclosure statement

No potential conflict of interest was reported by the author(s).

Funding

This work was supported by Javna Agencija za Raziskovalno Dejavnost RS: [Grant Numbers P4-0015 and P4-0430].

Data availability statement

The data presented in this study are available on request from the corresponding author.

ORCID

Daša Krapež Tomec http://orcid.org/0000-0003-1879-3830
Jure Žigon http://orcid.org/0000-0002-8326-0988
Miha Humar http://orcid.org/0000-0001-9963-5011
Mirko Karič http://orcid.org/0000-0002-8088-2570

References

Ayrilmis, N., et al., 2011. Effect of thermal-treatment of wood fibres on properties of flat-pressed wood plastic composites. *Polymer Degradation and Stability*, 96 (5), 818–822. doi:10.1016/j.polymdegradstab.2011.02.005.

Ayrilmis, N., et al., 2019. Effect of printing layer thickness on water absorption and mechanical properties of 3D-printed wood/PLA composite materials. *International Journal of Advanced Manufacturing Technology*, 102 (5–8), 2195–2200. doi:10.1007/s00170-019-03299-9.

Ayrilmis, N., Karič, M., and Kitek Kuzman, M., 2019. Effect of wood flour content on surface properties of 3D printed materials produced from wood flour/PLA filament. *International Journal of Polymer Analysis and Characterization*, 24 (7), 659–666. doi:10.1080/1023666X.2019.1651547.

Bučar, B., 2007. Internal and external moisture transport resistance during non-stationary adsorption of moisture into wood. *Zbornik Gozdarstva in Lesarstva*, 84, 17–21.

Cristian Neagu, R., et al., 2006. Ultrastructural features affecting mechanical properties of wood fibres. *Wood Material Science and Engineering*, 1 (3–4), 146–170. doi:10.1080/17480270701195374.

Ecker, J.V., et al., 2019. Mechanical properties and water absorption behaviour of PLA and PLA/wood composites prepared by 3D printing and injection moulding. *Rapid Prototyping Journal*, 25 (4), 672–678. doi:10.1108/RPJ-06-2018-0149.

European Standard – EN 323, 1993. *Wood-based panels. Determination of density*. Brussels: European Committee for Standardization (CEN).

Ezzaraa, I., et al., 2022. Micromechanical models for predicting the mechanical properties of 3D-printed wood/PLA composite materials: a comparison with experimental data. *Mechanics of Advanced Materials and Structures*, 29 (27), 6755–6767. doi:10.1080/15376494.2021.1983901.

Ezzaraa, I., et al., 2023. Numerical modeling based on finite element analysis of 3D-printed wood-polylactic acid composites: a comparison with experimental data. *Forests*, 14 (1), doi:10.3390/f14010095.

Galindo, S., and Ureña-Núñez, F., 2018. Enhanced surface hydrophobicity of poly(lactic acid) by Co60 gamma ray irradiation. *Revista Mexicana de Fisica*, 64 (1), 1–7. doi:10.31349/revmexfis.64.1.

Guo, R., et al., 2018. Effect of toughening agents on the properties of poplar wood flour/poly (lactic acid) composites fabricated with fused deposition modeling. *European Polymer Journal*, 107 (April), 34–45. doi:10.1016/j.eurpolymj.2018.07.035.

Hill, C.A.S., 2006. *Wood modification: chemical, thermal and other processes*. Chichester, England: John Wiley & Sons, 239.

Hill, C., Altgen, M., and Rautkari, L., 2021. Thermal modification of wood—a review: chemical changes and hygroscopicity. *Journal of Materials Science*, 56 (11), 6581–6614. doi:10.1007/s10853-020-05722-z.

Humar, M., et al., 2020. Quality control of thermally modified timber using dynamic vapor sorption (DVS) analysis. *Forests*, 11 (6), 1–12. doi:10.3390/f11060666.

Kain, S., et al., 2020. Effects of the infill pattern on mechanical properties of fused layer modeling (FLM) 3D printed wood/polylactic acid (PLA) composites. *European Journal of Wood and Wood Products*, 78 (1), 65–74. doi:10.1007/s00107-019-01473-0.

Kariz, M., et al., 2018. Effect of wood content in FDM filament on properties of 3D printed parts. *Materials Today Communications*, 14, 135–140. doi:10.1016/J.MTCOMM.2017.12.016.

Krapež Tomec, D., et al., 2021. Hygromorphic response dynamics of 3D-printed wood-PLA composite bilayer actuators. *Polymers*, 13, 3209. doi:10.3390/polym13193209.

Krapež Tomec, D., et al., 2023. Effect of thermal modification of wood particles for wood-PLA composites on properties of filaments, 3D-printed parts and injection moulded parts. *European Journal of Wood and Wood Products*, doi:10.1007/s00107-023-02018-2.

Križan, P., Beniak, J., and Matúš, M., 2020. Effect of wood particle size on the water absorption of wood-plastic composites. *Global Journal of Engineering and Technology Advances*, 5 (3), 069–079. doi:10.30574/gjeta.2020.5.3.0115.

Kutnar, A., et al., 2021. Viscoelastic properties of thermo-hydro-mechanically treated beech (Fagus sylvatica L.) determined using dynamic mechanical analysis. *European Journal of Wood and Wood Products*, 79 (2), 263–271. doi:10.1007/s00107-020-01629-3.

Kuzman, M.K., et al., 2019. Effect of selected printing settings on viscoelastic behaviour of 3D printed polymers with and without wood. *Materials Research Express*, 6 (10), doi:10.1088/2053-1591/ab411c.

Lazrak, C., et al., 2019. Structural study of maritime pine wood and recycled high-density polyethylene (HDPEr) plastic composite using Infrared-ATR spectroscopy, X-ray diffraction, SEM and contact angle measurements. *Case Studies in Construction Materials*, 10, e00227. doi:10.1016/j.cscm.2019.e00227.

Lee, S., et al., 2008. Thermal and mechanical properties of wood flour/talc-filled polylactic acid composites: effect of filler content and coupling treatment. *Journal of Thermoplastic Composite Materials*, 21, 209–223. doi:10.1177/0892705708089473.

Liu, X., et al., 2017. Effects of alkali treatment on the properties of WF/PLA composites. *Journal of Adhesion Science and Technology*, 31 (10), 1151–1161. doi:10.1080/01694243.2016.1248703.

Majka, J., Rogozinski, T., and Olek, W., 2022. Sorption and diffusion properties of untreated and thermally modified beech wood dust. *Wood Science and Technology*, 56, 1–17. doi:10.1007/s00226-021-01346-x.

Martikka, O., Kärki, T., and Wu, Q.L., 2018. Mechanical properties of 3D-printed wood-plastic composites. *Key Engineering Materials*, 777, 499–507.

Mazzanti, V., Malagutti, L., and Mollica, F. (2019) FDM 3D printing of polymers containing natural fillers: A review of their mechanical properties. *Polymers*, 11 (7), 1094.

Mazzanti, V., and Mollica, F., 2020. A review of wood polymer composites rheology and its implications for processing. *Polymers*, 12 (10), doi:10.3390/polym12102304.

NatureWorks, 2019. Technical data sheet of ingeo^{TM} biopolymer 2003D. *In*: *Technical data sheet* Minneapolis, MN: Natureworks B.V.), 4.

Nguyen, N.A., Bowland, C.C., and Naskar, A.K., 2018. A general method to improve 3D-printability and inter-layer adhesion in lignin-based composites. *Applied Materials Today*, 12, 138–152. doi:10.1016/j.apmt.2018.03.009.

Nussbaum, R.M., 1999. Natural surface inactivation of Scots pine and Norway spruce evaluated by contact angle measurements. *Holz Als Roh- Und Werkstoff*, 57 (6), 419–424. doi:10.1007/s001070050067.

Petrič, M., 2008. *Nelesni materiali v izdelkih lesnopredelovalne in pohištvene industrije*. Ljubljana: University of Ljubljana, Biotechnical faculty, Department of wood science, 148.

Petrič, M., and Oven, P., 2015. Determination of wettability of wood and its significance in wood science and technology: a critical review. *Reviews of Adhesion and Adhesives*, 3, 121–187. doi:10.7569/RAA.2015.097304.

Pohleven, F., and Rep, G., 2001. Wood modification – a promising method for wood preservation. *Drvna Industrija*, 52 (2), 71–76.

Rajendran Royan, N.R., et al., 2021. Current state and challenges of natural fibre-reinforced polymer composites as feeder in fdm-based 3d printing. *Polymers*, 13 (14), doi:10.3390/polym13142289.

Rep, G., Pohleven, F., and Kosmerl, S., 2012. Development of the industrial kiln for thermal wood modification by a procedure with an initial vacuum and commercialisation of modified Silvapro wood. In: *Proceedings of the 6th European Conference on Wood Modification*, *January 2001*, 11–17.

Segerholm, K., Ibach, R., and Wålinder, M., 2012. Moisture sorption of artificially aged wood-plastic composite. *BioResources*, 7, 1283–1293. doi:10.15376/biores.7.1.1283-1293.

Stoof, D., Pickering, K., and Zhang, Y., 2017. Fused deposition modelling of natural fibre/polylactic acid composites. *Journal of Composites Science*, 1 (1), doi:10.3390/jcs1010008.

Straže, A., 2010. *Vpliv notranjega in zunanjega snovnega upora na kinetiko konvekcijskega sušenja lesa, Impact of internal and external mass transfer resistance on kinetics of convective wood drying*. Doctoral dissertation, University of Ljubljana, Biotechnical faculty, 114p*TA instruments*. (n.d.). https://www.tainstruments.com/applications-notes/introduction-to-dynamic-mechanical-analysis-and-its-application-to-testing-of-polymer-solids/.

Tao, Y., et al., 2017. Development and application of wood flour-filled polylactic acid composite filament for 3D printing. *Materials*, 10 (4), 339. doi:10.3390/ma10040339.

Tao, Y., et al., 2021. A review on voids of 3D printed parts by fused filament fabrication. *Journal of Materials Research and Technology*, 15, 4860–4879. doi:10.1016/J.JMRT.2021.10.108.

Unterweger, C., et al., 2018. 3D computed tomography as Quality Control Tool in Advanced Composite Manufacturing. In: *8th Conference on Industrial Computed Tomography*, Wels, Austria (ICT 2018), *February*, 1. https://www.researchgate.net/publication/323552184.

van de Werken, N., et al., 2020. Additively manufactured carbon fiber-reinforced composites: state of the art and perspective. *Additive Manufacturing*, 31, 100962. doi:10.1016/J.ADDMA.2019.100962.

Wang, X., et al., 2019. Effect of porosity on mechanical properties of 3D printed polymers: experiments and micromechanical modeling based on X-ray computed tomography analysis. *Polymers*, 11 (7), doi:10.3390/polym11071154.

Yan, Z.L., et al., 2013. Fabrication process optimization of hemp fibre-reinforced polypropylene composites. *Journal of Reinforced Plastics and Composites*, 32 (20), 1504–1512. doi:10.1177/0731684413501925.

Yue, Z., et al., 2022. Mechanical, thermal and rheological properties of polylactic acid (PLA)/epichlorohydrin modified pine wood flour (EWF) composites. *European Journal of Wood and Wood Products*, 80 (5), 1111–1120. doi:10.1007/s00107-022-01810-w.